


FULL PAPER

Open Access



Variations of crustal thickness and average Vp/Vs ratio beneath the Shanxi Rift, North China, from receiver functions

Yifang Chen^{1*} , Jiuhui Chen¹, ShunCheng Li¹, Zhanyang Yu², Xuzhou Liu³ and Xuzhang Shen²

Abstract

The Shanxi Rift located in the central part of the North China Craton (NCC) as a boundary between the Ordos block and the Huabei basin. The Shanxi graben system is a Cenozoic rift and originated from back-arc spreading related to westward subduction of the western Pacific and far field effects caused by northward subduction of the Indian plate. It has also had strong earthquake activity in China since the Quaternary. To investigate the tectonic evolution and tectonic setting of strong earthquakes in the Shanxi Rift, we apply the receiver function $H\text{-}\kappa$ stacking method to determine the crustal thickness and average Vp/Vs ratio in the area. The results show that the thickness of the crust increases from approximately 30 km in the Huabei basin to approximately 47 km in the Yinshan Mountains with a close correlation between the Moho depth and topography. The Yuncheng, Linfen and Taiyuan grabens have varying degrees of crustal thinning. The crustal average Vp/Vs ratio in the Shanxi Rift has significant heterogeneity; the high Vp/Vs ratio (~ 1.85) are found in the Datong and Yuncheng grabens, and Vp/Vs ratio of the Taiyuan and Linfen grabens is approximately 1.75 which close to the global average value ~ 1.782 . Combining the observations in this study with previous research, we suggest that the grabens in the Shanxi Rift experienced extensional deformation from south to north and that the possibility of strong earthquakes in the central part of the Shanxi seismic belt is greater than that on the northern and southern sides.

Keywords: Shanxi Rift, Receiver function, $H\text{-}\kappa$ stacking, Crustal thickness, Vp/Vs ratio

Introduction

The Shanxi Rift is a famous terrestrial rift system and is located in the Trans-North China Orogen (TNCO). The TNCO was assembled ~ 1.85 Ga ago (Zhao et al. 2001) and is bounded by the Ordos block in the western North China Craton (NCC) to the west and by the Huabei basin in the eastern NCC to the east. The Ordos block is a stable craton with minor internal deformation and has a counterclockwise rotation caused by the north-eastward growth of the northeastern Tibetan Plateau (Deng et al. 1999; Yin 2000; Tapponnier et al. 2001). The

Huabei basin, as part of the eastern North China Craton, has undergone intensive lithospheric extension and destruction, and offset rift basins have formed, which are induced by the westward subduction of the Pacific plate and the India–Asia collision (Northrup et al. 1995; Tian et al. 1992; Liu et al. 2007; Chen et al. 2009; Zhu et al. 2012). The Shanxi Rift, as a transition zone between the Ordos block and Huabei basin, is adjacent to two units with distinct tectonic patterns and is located in a complex tectonic environment.

The Shanxi Rift has undergone multistage extensional deformation during the late Cenozoic and is still undergoing extensional deformation today (Deng et al. 1973; Tapponnier et al. 1982; Xu et al. 1993; Shen et al. 2000; Zhang et al. 1998, 2003; Shi et al. 2015). However, the rifting mechanism of the Shanxi Rift remains controversial.

*Correspondence: yifangchen_9134@hotmail.com

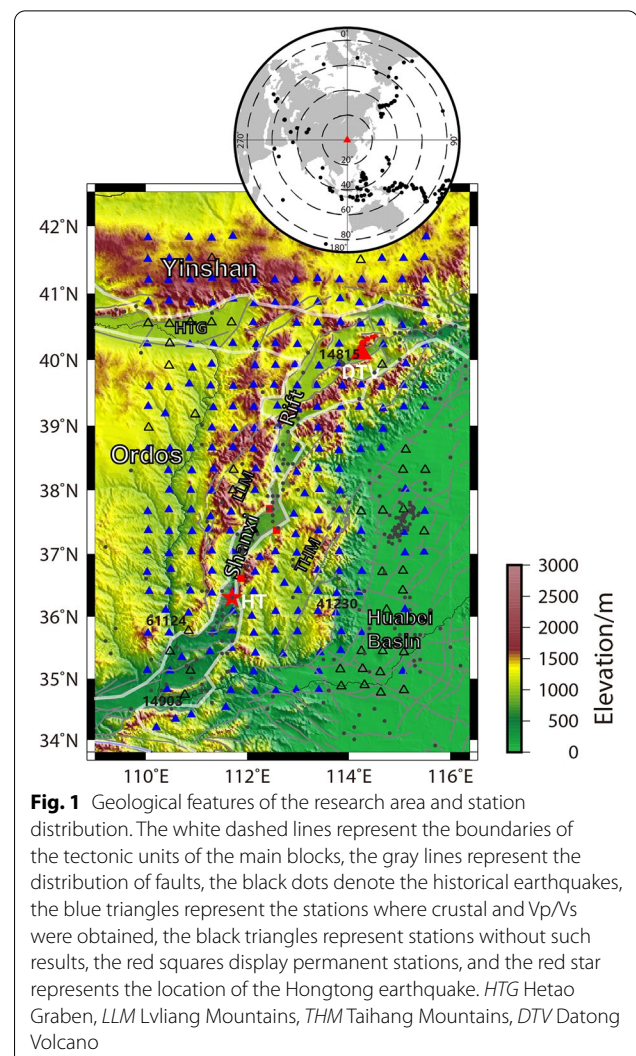
¹ Lhasa National Geophysical Observation and Research Station, State Key Laboratory of Earthquake Dynamics, Institute of Geology, CEA, Beijing 10029, China

Full list of author information is available at the end of the article

Some researchers have argued that the evolution of the Shanxi Rift has been dominated by regional stress fields formed by the collision of India and Eurasia (Tapponnier and Molnar 1976; Xu and Ma 1992); some researchers have proposed that the Shanxi Rift was formed by mantle plume upwelling from the lower mantle (Zhao et al. 2011; Lei 2012), while others have argued that, based on many studies of tectonic properties in the Shanxi Rift from north to south in recent years, the rifting mechanisms in the southern and northern Shanxi Rift are different (Song et al. 2012; Tang et al. 2013; Ai et al. 2019; Su et al. 2021; Cai et al. 2021). Thus, the Shanxi Rift and its adjacent regions are a key region for understanding the tectonic evolution of the NCC and regional rift dynamics study.

The western and eastern boundaries of the Shanxi Rift are defined by the Lvliang Mountains and the Taihang Mountains, respectively (Fig. 1). Its northern and southern sides are connected by the E–W-trending Hetao graben and the Weihe basin. The Shanxi Rift system is composed of the Datong, Xinding, Taiyuan, Linfen and Yuncheng basins and is bounded by normal and strike–slip faults, which form an S-shaped feature over a distance of ~1200 km (Xu and Ma 1992; Li et al. 1998; Zhang et al. 1998). The Shanxi Rift is also a large active fault zone and has experienced destructive historical earthquakes (e.g., the 1303 Hongtong M_S 8.0 earthquake and the 1695 Linfen M_S 7³/₄ earthquake). Therefore, studying the deep physical structure in the area can provide important information for understanding the mechanism of strong earthquakes and the seismogenic background beneath the Shanxi Rift.

In recent years, many geophysical studies of deep structures have been conducted in the Shanxi Rift and surrounding regions. Local earthquake traveltime tomographic (Chang et al. 2007), joint inversion of surface waves and gravity anomalies (Guo et al. 2015) and surface wave tomography (Song et al. 2015) indicates that the crustal P-wave and S-wave velocity structures of the Shanxi Rift and its surrounding regions are heterogeneous, the upper crust of the Yuncheng and Linfen basins in the south of the rift is dominated by lower velocity, while the lower crust is characterized by higher velocity; the middle and lower crust of the Datong Basin in the north is characterized by low velocity. The results of electrical conductivity studies also show that significant lower-resistivity anomalies exist in the middle and lower crust of Datong volcano based on the three-dimensional magnetotelluric inversion technique (Zhang et al. 2016). Tang et al. (2010) and Li et al. (2014) used the receiver function migration and seismic reflection method and found that the Moho interface exhibits uplift beneath the Shanxi Rift to varying degrees. To consider the thinning phenomenon of



the crust beneath the Shanxi Rift, Liu et al. (2011) and Li et al. (2010) obtained controversial results using the receiver function method. Li et al. (2010) found that the basement structure is well-preserved and the crust is relatively thick. Liu et al. (2011) revealed that the crustal thickness of the south Shanxi Rift is significantly 5 to 10 km shallower than the surrounding areas. However, previous studies are based on sparse permanent seismic stations or linear temporary seismic arrays which is difficult to obtain high-resolution image or complete understanding in the area.

In this paper, we used the teleseismic waveforms from the seismic stations of the China Array seismic experiment phase III (ChinArray 2006) and applied the receiver function H - κ stacking technique (Zhu and Kanamori 2000) to obtain the crustal thickness and average V_p/V_s ratios in the Shanxi Rift and surrounding

regions. By integrating seismic structural images with previous research results, we attempt to discuss and analyze the tectonic evolution of the Shanxi Rift and seismogenic environments beneath the Shanxi seismic belt.

Data and method

Data

Teleseismic waveform data recorded from the China Array seismic experiment during 2016–2018 are used in this study. We obtained data from approximately 230 broadband seismic stations that almost evenly cover the eastern margin of the Ordos block, the Shanxi Rift, the Taihang Mountains and the western margin of the Huabei basin with station spacing of 30–50 km (Fig. 1). Earthquake waveforms with magnitudes $M_s > 5.5$ and epicentral distances of 30–90 degrees were used to compute the P-wave receiver function (Fig. 1).

Receiver functions and the H - κ stacking technique

The P-wave receiver function (PRF), which is based on the source-equalization assumption, is defined as the impulse response of the crust and upper mantle structure beneath the seismic station to the direct P-wave from the teleseismic waveform (Langston 1979; Farra and Vinnik 2000). The receiver function is an indispensable tool that is widely used to image the deep structure of the crust and upper mantle (Kind et al. 2002; Yuan et al. 2006; Liu et al. 2014). Coordinate rotation and deconvolution are the two main steps to calculate and obtain the receiver function (Ammon 1991; Liu et al. 1996). The original waveform was rotated from the ZNE (vertical, north–south, east–west) coordinate system to the ZRT (vertical, radial, tangential) coordinate system and was filtered with a Gaussian width factor of 5.0. Then, we computed the PRFs after deconvolving the Z component from the R component in frequency domain (Liu et al. 1996). All isolated PRFs were filtered with a Butterworth band filter of 0.05–1 Hz. Every trace of receiver function was checked to ensure that only high-quality data were used in this study.

The crustal thickness and average Poisson's ratio, as crucial parameters describing the physical characteristics of the crust, have been important seismic evidence in geodynamics research. Zandt and Ammon (1995) used the arrival time relationship between the P_{ms} phase and multiple PpP_{ms} phase to study the global variation in Poisson's ratio determined uniquely from the ratio of P- and S-wave velocities. Zhu and Kanamori (2000) developed the H - κ stacking technique, which can extract the thickness of the crust and the ratio of P- and S-wave velocities (Vp/Vs ratio) beneath a station by constructing an H - κ grid and stacking (Fig. 3):

$$S(H, \kappa) = w_1 r(t_{Ps}) + w_2 r(t_{PpPs}) - w_3 r(t_{PsPs+PpSs}). \quad (1)$$

Here, w_1 , w_2 and w_3 are the weighting coefficients of amplitudes (r) of the Moho conversion Ps, reverberated PpPs and PsPs+PpSs phases, which are 0.6, 0.25, and 0.15 in this study. According to a grid search of the maximum stacking energy (S) of the weighted receiver function amplitudes (Ps, PpPs and PsPs+PpSs), we can obtain the thickness of the crust (H) and the average Vp/Vs ratio (κ) in the H - κ grid.

A loose sedimentary layer beneath a seismic station induces a delayed arrival time of the converted and multiple phases in the receiver function (Luo et al. 2008; Yeck et al. 2013; Yu et al. 2015), which may cause bias to the estimation of the crustal thickness and average Vp/Vs ratio using the H - κ stacking technique. The distribution of sedimentary thicknesses in the study area (Fig. 2) shows that low-velocity sediments with a thickness of a maximum of 3 km are covered in the central Ordos, Shanxi Rift and part of the Taihang Mountains, which may lead to a deviation in the results. Here we try to reduce the influence (time delay) of the sediment layers on the H - κ stacking by correcting the travel time for the sediment layer. After subtracting the travel times of conversion Ps, reverberated PpPs and PsPs+PpSs in sediment layers (can be calculated according to the obtained velocity model) and applying the H - κ stacking, we will get more accurate information of crustal thickness and average Vp/Vs ratio. However, the larger impedance contrast of the sediment–crust interface can produce stronger amplitude reverberations in the RFs that frequently masking the Ps phases from Moho and completely blurring the result of H - κ stacking. In this case the time correction for the sediment layer may not work. To examine the applicability of time correction for sediment layer in different situations, we have conducted extensive synthetic tests with different thickness and Vp/Vs for the sediment layer (Additional file 1: Figure S1–S6). According to the tests we found that the presence of the sedimentary layer with thicker thickness or larger Vp/Vs ratio can produce larger reverberations that strongly interfere with signals of Moho and multiples in RFs and make the H - κ stacking unapplicable (Additional file 1: Figure S5b–c). Combining with the distribution of sedimentary thicknesses and Vp/Vs ratio in Fig. 2, we know that the data of station in most areas can be used in the study.

To evaluate the impact of the low-velocity sedimentary layer in research region on the estimation of the crustal thickness and average Vp/Vs ratio by using receiver function H - κ stacking, we constructed a two-layer crustal model with a 3-km-thick sedimentary layer (the structure of the sedimentary layers below station 61124 in

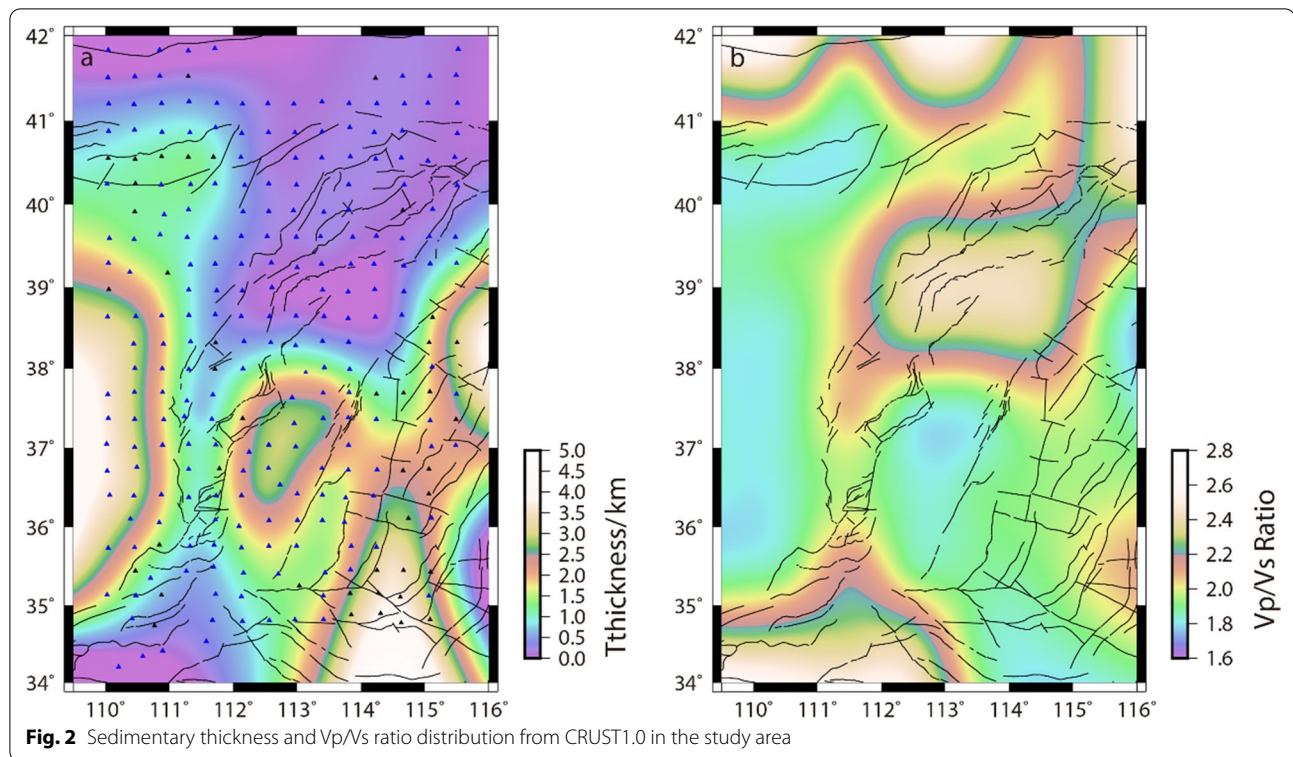
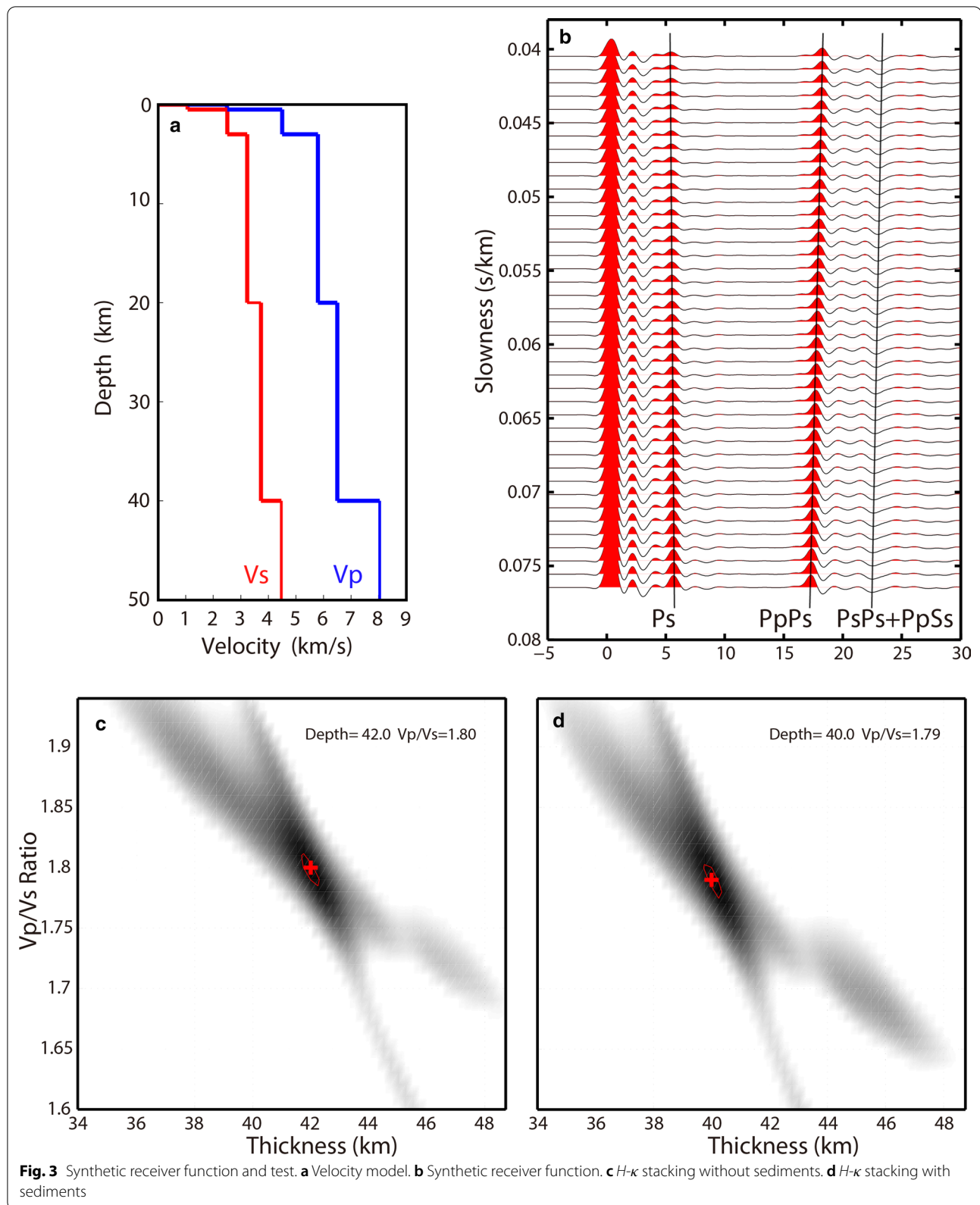


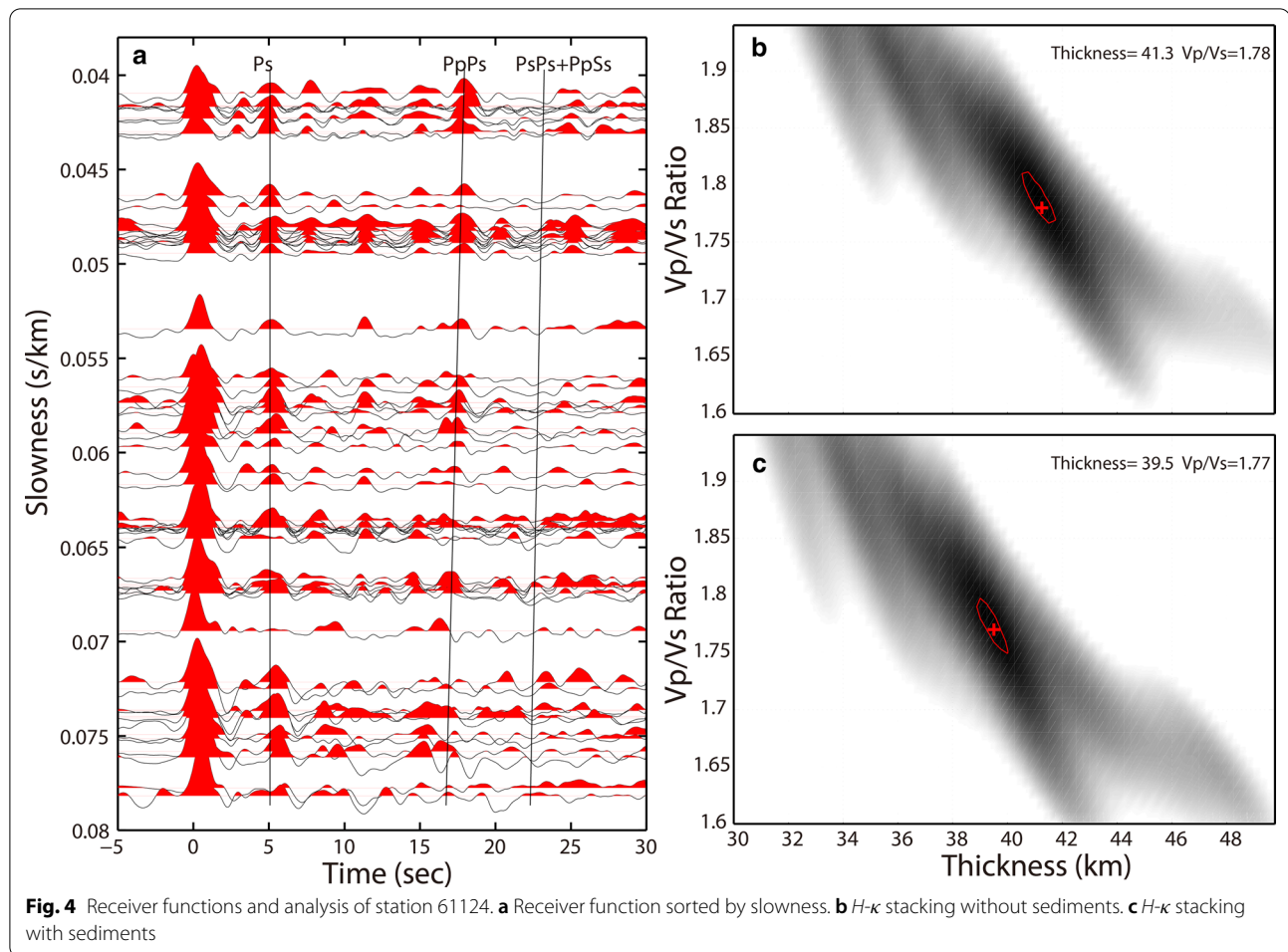
Fig. 1 were obtained from CRUST1.0). The thickness and the P-wave and S-wave velocities of the upper and lower sedimentary layers are 0.5 km, 2.50 km/s, and 1.07 km/s and 2.5 km, 4.50 km/s, and 2.51 km/s, respectively; the average Vp/Vs ratio of the crust below the sedimentary layer is 1.78, and the crustal thickness is 40 km (Fig. 3a). We calculate the synthetic PRF seismograms (Fig. 3b) of the velocity model (Fig. 3a) with slowness in the range of ~ 0.04 to ~ 0.077 s/km by using the generalized reflection–transmission coefficient matrix method (Chen 1993). The results of H - κ stacking analysis without correcting the arrival time in sedimentary layers show that the crustal thickness has a deviation of 2 km and that the Vp/Vs ratio is also influenced (Fig. 3c). After considering the time delay resulted from sedimentary layers, the results obtained by the receiver function are closer to the real crustal thickness and the average Vp/Vs (Fig. 3d). Next, we use data from station 61124 for testing (Fig. 4). Figure 4a displays the PRFs of station 61124 sorted by slowness in the time domain, and it shows that the arrival times of converted (P_m s) and multiple phases (PpP_m s and PpS_m s + PpS_m s) are ~ 5 s, ~ 16.8 – ~ 17.9 s and ~ 22.3 – ~ 23.2 s, respectively. A comparison of the results of the receiver function H - κ stacking analysis in Fig. 4b and c show that the estimation of the crustal thickness without correcting for sedimentary layers has a deviation of a maximum of 1.8 km and that the average Vp/Vs

ratio has also been influenced. Therefore, the reliable result of the crustal thickness and average Vp/Vs ratio, which are closer to the actual situation in the research region, would be obtained by applying receiver function H - κ stacking after correcting for the time delay in sedimentary layers. It is important to note that although the CRUST1.0 is the latest global crustal model based on the previous results of active and passive source seismic detection and it still has some uncertainty. The sedimentary thickness distribution of CRUST1.0 in most areas of our research region is in good agreement with the previous results (Wang et al. 2017; Wu et al. 2018), except for the Hetao graben which has the sedimentary layer with a thickness > 5 km (Teng et al. 2008). So it is necessary to judge whether it is applicable based on the quality of real data.

Results

In this study, we obtain the crustal thickness and average Vp/Vs ratio of 217 seismic stations based on the receiver function H - κ stacking technique by correcting for the time delay from the loose sedimentary layers (velocity structure extracted from CRUST1.0). The data from the remaining stations (black triangles in Fig. 1) are not reliable due to the lack of receiver functions or stronger reverberation caused by the larger impedance contrast of the sediment–crust interface (e.g., stations



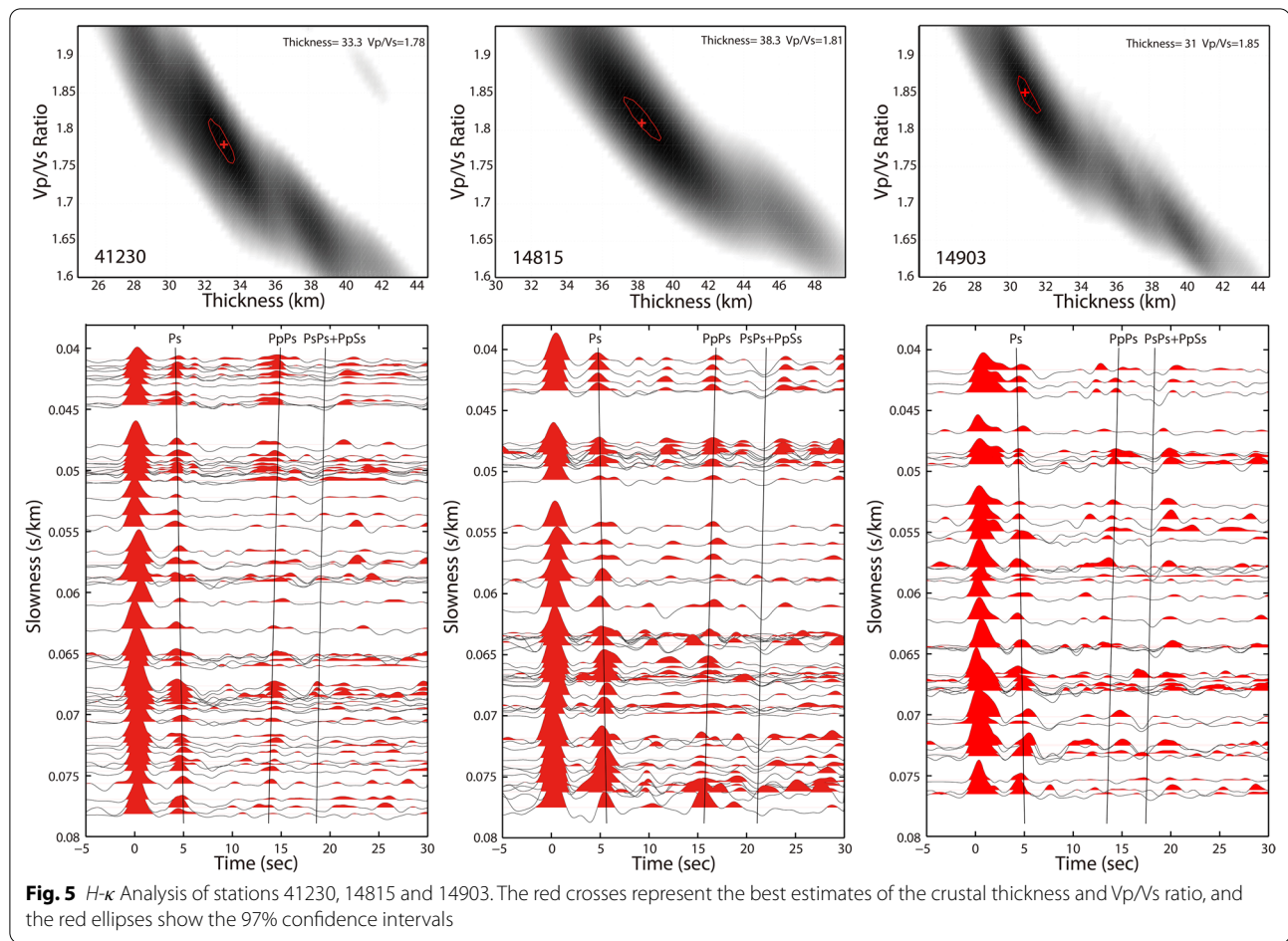


41210 and 15782 are shown in Additional file 1: Figure S7). We also included the results from permanent stations JIC, TAG and HZH (red squares in Fig. 1) as a supplement to enhance the reliability of the results in some areas (He et al. 2014). Figure 5 illustrates examples of the P receiver functions and results from the H - κ analysis at stations 41230, 14815 and 14903, and the obtained distributions of the crustal thickness and average Vp/Vs ratio are shown in Fig. 6. The overall uncertainties are ± 0.3 – 1.6 km for crustal thickness and ± 0.01 – 0.09 for κ at each station (Additional file 1: Table S1).

Figure 6a shows that the crustal thickness of the study area gradually increases from the southeast to the northwest, from approximately 30 km to approximately 47 km. Thinner crust of 30–37 km is observed on the east side of the 37 km contour (the blue line in Fig. 6a), which is in good agreement with the north–south gravity lineament (the white dashed line in Fig. 6a). To the west of the 37 km contour, the crustal thicknesses of the Taihang Mountains and Lvliang Mountains are 37–42 km and 37–45 km, respectively; the crustal thickness of the stable

Ordos block is 39–43 km, and the thickest crustal thickness of 43–46 km is observed in the Yinshan Mountains. The crustal thickness distribution in the Shanxi Rift varies significantly from south to north, ranging from 32 to 38 km in the Yuncheng graben and the southern Linfen graben, 36–38 km in the Taiyuan graben, and approximately 42 to 43 km in the other grabens. A comparison of the crust thickness from Ai et al. (2019) based on joint inversion of receiver functions and surface waves reveal that our result clearly shows the better correlation with geological features in the research region (e.g., the Yuncheng, Linfen and Taiyuan grabens have varying degrees of crustal thinning; the 37 km contour line divides the TNCO and the eastern NCC), which attributed to the denser array used in the paper.

In the study region, H - κ stacking results reveal crustal Vp/Vs ratios between 1.63 and 1.92, with an average value of approximately 1.79 (Fig. 6a), which is close to the global continental average Vp/Vs ratio of 1.782 (Zandt and Ammon 1995). Higher Vp/Vs ratios are observed in the Yuncheng and Datong grabens and



from the northern Ordos block to the Yinshan Mountains, with an average value of 1.85. The average V_p/V_s ratios of the northern Linfen graben and the Taiyuan graben are approximately 1.75, and those of the central Ordos block and from the Huabei basin to the Taihang Mountains are 1.72–1.76 and 1.63–1.75, respectively. The V_p/V_s ratio of the northern Ordos block reaches 1.86. Tian et al. (2011) also observed a high anomaly in the V_p/V_s ratio by receiver functions and argued that lower crustal ductile flows transfer from the Hetao graben to the northern Ordos Block. The variations in the crustal thickness and V_p/V_s ratios obtained in this paper are in good agreement with the published results based on receiver function velocity inversion, discontinuity imaging, H - κ stacking techniques and deep seismic sounding (DSS) method (Chen et al. 2009; Zheng et al. 2009; Tang et al. 2010; Wei et al. 2013; He et al. 2014; Li et al. 2014; Wang et al. 2014). However, more densely distributed seismic stations are used in this paper; therefore, our results should have a higher resolution.

Discussion

Moho depth and relief

The correlation between the Moho depth and topography provides information on gravitational isostatic equilibrium, which can help in the understanding of the tectonic evolution of the research region. Linear fitting revealed that the linear regression equation between the depth of the Moho (H) and the elevation (E) is $H = 5.51E + 32.48$, and the correlation coefficient is $R \approx 0.7$ (Fig. 7a). The slope between the Moho depth and elevation is ~ 5.51 (also called the isostasy coefficient), which is much greater than the typical continental crust value of 4.45 (Guo et al. 2012). As shown in Fig. 7b, the slope between the Moho depth and elevation in southern and northern Shanxi rift and its adjacent regions is 4.77 and 5.36, respectively. According to the AIRY equilibrium theory, the larger slope is caused by the smaller density difference between the crust and the mantle (Airy 1855). As shown in Fig. 5, the multiple wave (PpP_ms) of the RFs of station 14903 (located in Yuncheng graben) is characterized by multi-peak, which means that the Moho beneath the station may possibly be a velocity transitional zone

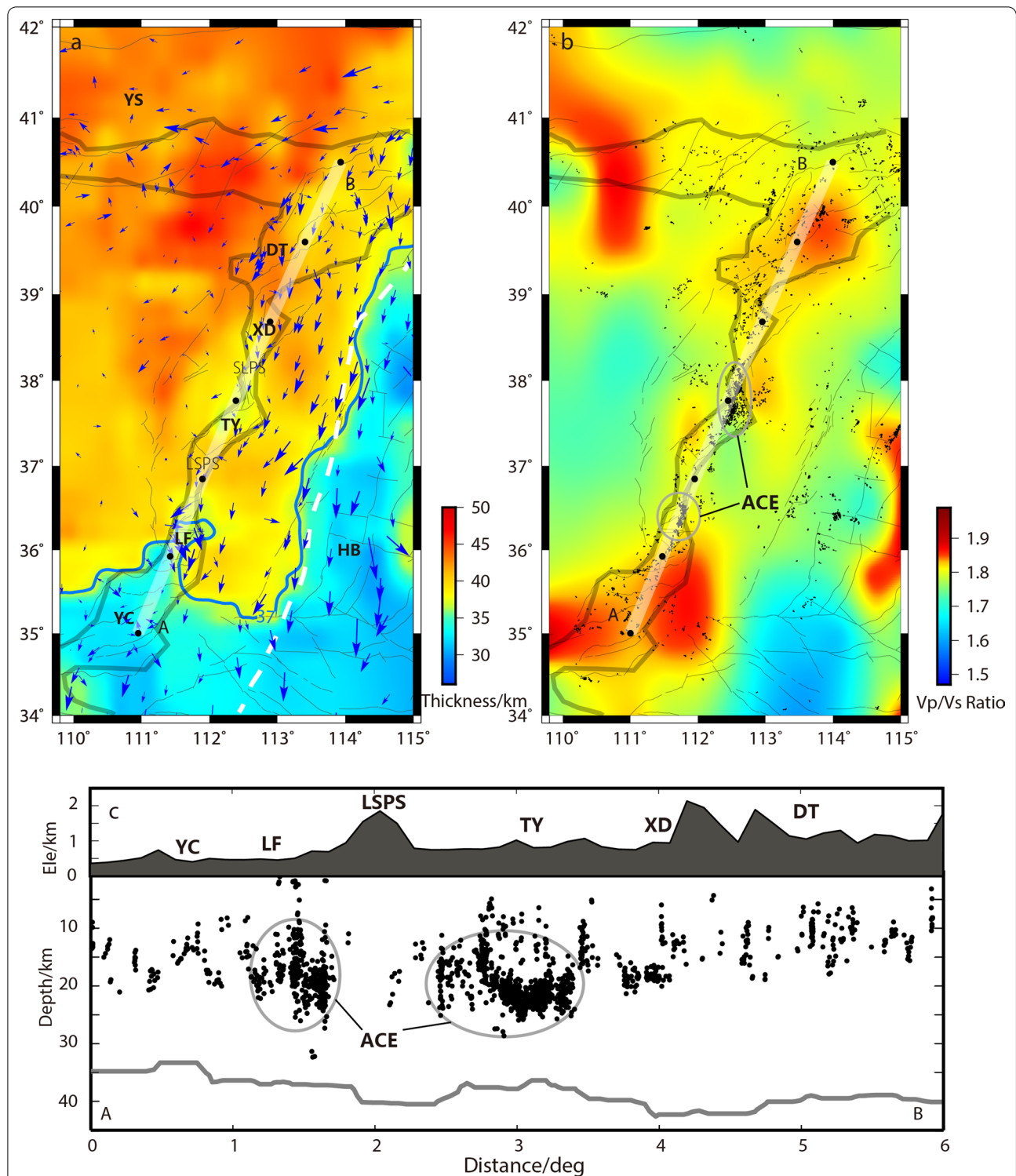
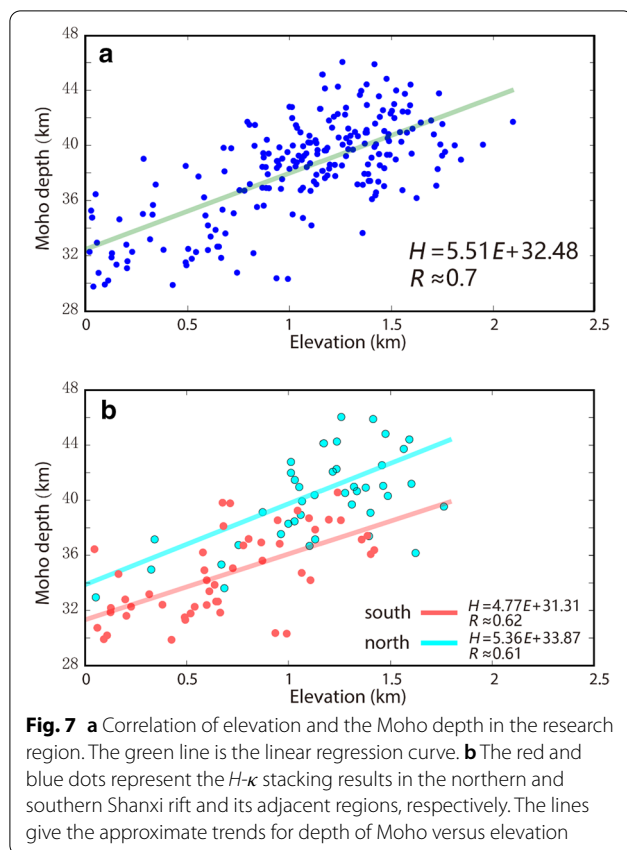


Fig. 6 Crustal thickness, Vp/Vs ratio and earthquakes distribution in the research area. **a** Crustal thickness. **b** Vp/Vs ratio. **c** Seismicity pattern along the Shanxi Rift shown in **b**. The blue arrows display GPS velocity vectors; the black dots represent the locations of earthquakes, the white dashed line indicates the north-south gravity lineament, and the gray line stands for the crustal thickness along the profile AB. YC Yuncheng graben, LF Linfen graben, TY Taiyuan graben, XD Xinding graben, DT Datong graben, YS Yinshan Mountains, HB Huabei basin, LSPS Lingshi Push-up Swell, SLPS Shilingguan Push-up Swell, ACE area with concentrated distributions of earthquakes



based on the test of synthetic RF (the velocity model with a transitional Moho) in Fig. 8. The Bouguer gravity data reveal that there are significant gravitational anomalies beneath the Shanxi Rift that are characterized by gravity values in the -120 to -145 mGal range (Xu and Ma 1992). Wang et al. (2001) obtained relatively high heat flow values in the Shanxi Rift, which has an average heat flow of 68 ± 10 mWm $^{-2}$. Combining these results, we speculate that there may be an exchange of materials and energy between the crust and mantle below the Shanxi Rift and its adjacent regions and the northern part is more intense than the southern part.

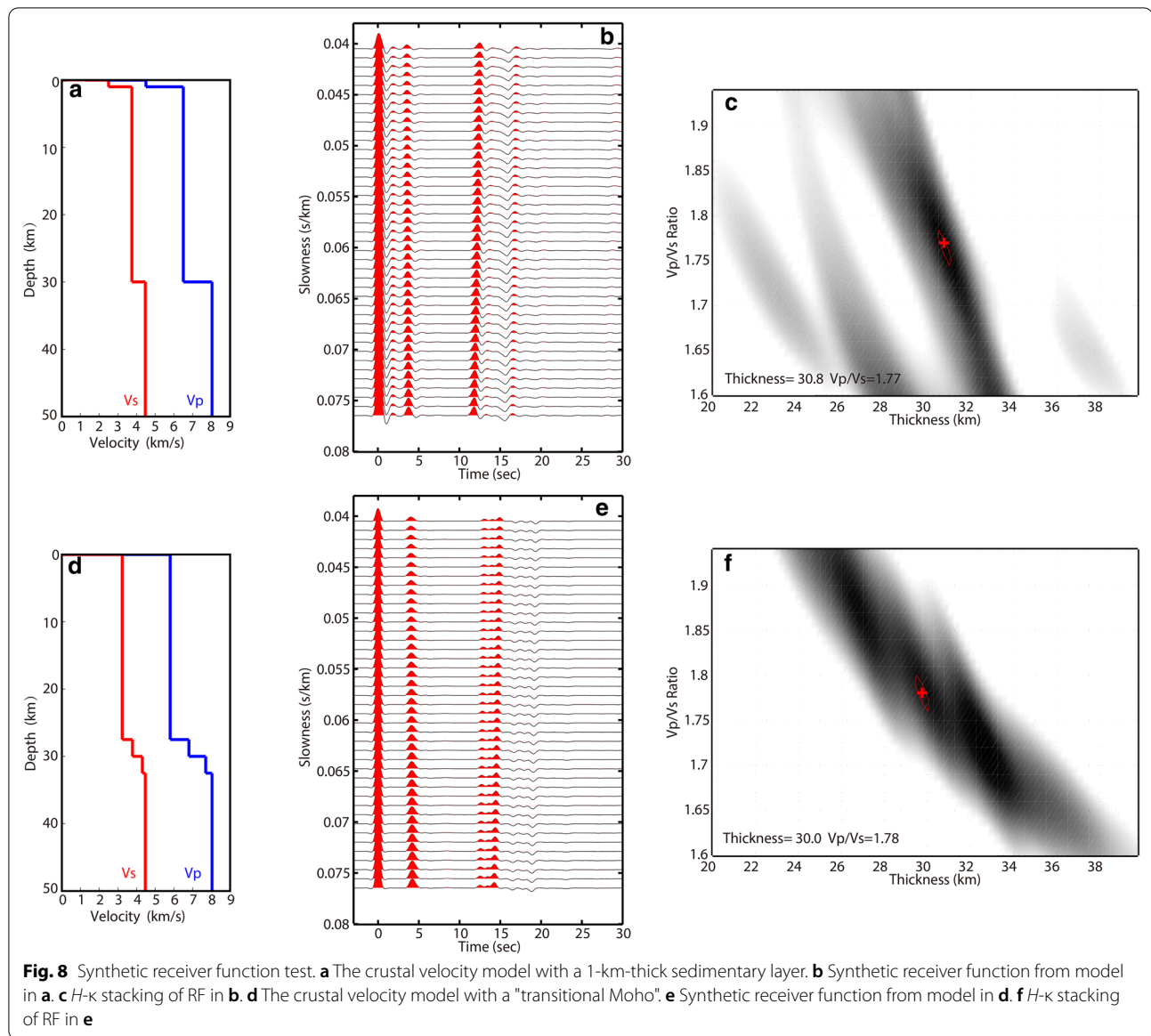
Crustal thickness and north–south difference in the Shanxi Rift

The term rift refers to the initial stage of continental break-up, where continuous development may lead to the rupture of the lithosphere and the formation of new ocean basins. A rift, as an extensional tectonic unit bounded by normal faults, has obvious lithospheric anomalies, which usually manifested as a thinned crust and mantle upwelling, and has often been described by two end-member models, active rifting and passive rifting (Sengör and Burke 1978; Olsen 1995; Kearey et al. 2009). Active rifting is defined as rifting in response to

a thermal upwelling of the mantle and characterized by lithospheric velocity anomalies. Passive rifting is defined as rifting in response to a regional stress field, usually assumed to originate from remote plate boundary forces (the lithosphere is thinned only in response to extension). However, there is still insufficient understanding of the crustal structure of the Shanxi Rift.

The images of Moho depth obtained by Tang et al. (2010) using the receiver function migration technique show that there is obvious uplift of the Moho approximately 4–6 km below the Taiyuan and Linfen grabens. Fine crustal structures obtained by Li et al. (2014) with the DSS method showed that the Moho interface was uplifted approximately 3 km beneath the Linfen graben. However, the above results are based on two-dimensional profiles. The crustal structure results in this paper can provide more specific information for the crustal thickness variation in detail below the Shanxi Rift, which reveals that there are Moho uplift of 6–8, 3–5, and 2–4 km below the Yuncheng, Linfen and Taiyuan grabens. The Yuncheng graben has the most obvious crustal thinning, followed by the Linfen and Taiyuan grabens. The crustal thinning feature between the Taiyuan and Linfen grabens is separated by the Lingshi Push-up Swell at the southern end of the Taiyuan graben. The Xinding and Datong grabens, which are in the northern part of the Shanxi Rift, have no crustal thinning, which is consistent with the Moho depth obtained by using receiver functions migration (Chen et al. 2009; Cheng et al. 2013).

GPS-based research by Shen et al. (2000) showed that the Shanxi Rift has an extensional rate of approximately 4 ± 2 mm/year. The dense GPS velocity field with respect to the Ordos block shows that the Taihang Mountains move southward at a rate of 1.2 mm/year, causing dextral shear across the Shanxi grabens, and the Yuncheng graben located in the southern Shanxi graben has a dextral slip rate of 0.8 ± 0.1 mm/year and an extensional rate of 0.9 ± 0.1 mm/year (Hao et al. 2021), which are consistent with the tectonic background stress and main types of earthquake mechanisms in the region (Sheng et al. 2015; Qu et al. 2017). Tang et al. (2013) and Ai et al. (2019) used the joint inversion of ambient noise and surface waves and the joint inversion of receiver functions and surface waves to obtain the S-wave velocity structure of the crust and upper mantle in the region, indicating that there are significant differences between the northern and southern sides of the Shanxi Rift. In the upper crust of the southern Shanxi Rift, the Yuncheng, Linfen, and Taiyuan grabens are dominated by low-velocity anomalies, while the Datong and Xinding grabens in the north are characterized by high-velocity anomalies; from the middle and lower crust to the upper mantle, the Datong graben exhibits a lower velocity structure, while the



Yuncheng and Linfen grabens are dominated by higher anomalies. Combining the isostasy coefficient obtained in Fig. 7b, we argue that the grabens in the southern and central parts of the Shanxi Rift are less affected by deep mantle upwelling than the grabens in the northern parts of the Shanxi Rift, and the current extensional deformation and depression are mainly due to regional tensional stresses. The extensional environment is due to different rates of the motion of blocks (around the Shanxi Rift) along the strike-slip boundary, which may be caused by back-arc spreading of the Pacific Plate and pushing of the northeastern Tibetan Plateau since the Mesozoic. The low-temperature thermochronology results obtained by Su et al. (2021) imply that the development of grabens in

the southern Shanxi Rift occurred earlier than that in the central and northern regions. Combining previous studies and the crustal thickness variation obtained in this paper, we speculate that the grabens in the Shanxi Rift have experienced a gradual development process from south to north, corresponding to the most obvious feature of crustal thinning in the Yuncheng graben, followed by the Linfen and Taiyuan grabens.

Variation in the V_p/V_s ratio and seismogenic environment

Poisson's ratio plays a vital role in studying the composition of crustal materials and is an important elastic parameter reflecting the shear deformation potential in crust (Zandt and Ammon 1995; Christensen et al. 1996).

Poisson's ratio can be determined uniquely from the V_p/V_s ratio, $\sigma = 0.5 \times [1 - 1/(\kappa^2 - 1)]$, which show a positive correlation. The upper crust is enriched in felsic rocks with lower Poisson's ratios (<0.26), and the lower crust is dominated by mafic materials with higher Poisson's ratios (>0.28); when Poisson's ratio is greater than 0.3, the lower crust may be partially molten or fluid (Zandt and Ammon 1995). This demonstrates that the material with the larger V_p/V_s ratio (or Poisson's ratio) is more prone to shear deformation (Christensen and Fountain 1975). The variation in the V_p/V_s ratio in this paper shows that there are significantly higher anomalies in the Yuncheng and Linfen grabens of the southern Shanxi Rift and in Datong volcano of the northern Shanxi Rift. According to the velocity structure research mentioned above (Chang et al. 2007; Tang et al. 2013; Ai et al. 2019), we argue that the higher V_p/V_s ratios in the Yuncheng graben and the southern Linfen graben are caused by the low velocity of the upper crust, which verifies that the deformation of the upper crust results from a tensional environment in this region. The higher V_p/V_s ratio beneath Datong volcano corresponds to the lower-velocity and lower-resistivity structures in the middle and lower crust in the region (Zheng et al. 2009; Zhang et al. 2016), which may be related to the magmatic activity of mantle upwelling.

An accurate relocation of the earthquake (black dots in Fig. 6b, c) in the Shanxi seismic belt is obtained by using the double difference relocation algorithm from the integrated travel time data recorded at the permanent seismic stations during 2009–2018, and it is in good agreement with the results of Song et al. (2012) and Wang et al. (2020). As shown in Fig. 6b and c, we find that the distribution and focal depths of earthquakes are correlated with the variation in the V_p/V_s ratio in the Shanxi Rift. From the perspective of epicenter distribution, a comparison of the discretely distributed earthquakes in the Datong, Xinding and Yuncheng grabens reveals that there are two areas with significantly concentrated distributions of earthquakes (ACE) in the northern Taiyuan graben and the northern Linfen graben, which correspond to the abrupt belt of variation in the V_p/V_s ratio in Fig. 6b and c (earthquakes mainly occur in the region characterized by a lower V_p/V_s ratio). Wang et al. (2009) also found the same feature of earthquake distribution by researching Poisson's ratio in the Capital Circle Region. In terms of focal depth, earthquake depths in the Datong, Xinding and Yuncheng grabens are basically above 20 km, yet a large number of earthquakes with focal depths of 20–30 km exist in the ACE (Fig. 6c). It is worth noting that both the Hongtong M_s 8 earthquake and the Linfen M_s 7.4 earthquake occurred in the region with both high V_p/V_s ratios and low V_p/V_s ratios in the

Linfen graben. This corresponds to the large value of the GPS displacement field (blue arrows in Fig. 6a) (Hao et al. 2021). As mentioned above, a region with a larger Poisson's ratio is more easily deformed, and a region with a low Poisson's ratio is more likely to accumulate energy and cause destructive earthquakes, which explains the above phenomenon. Moreover, through studying the Changning seismicity area, Hu et al. (2021) found that the lateral difference in Poisson's ratio is probably the main cause of the local difference in the stress field. Therefore, we believe that the possibility of strong earthquakes in the Taiyuan and Linfen grabens in the central Shanxi Rift is greater than in the grabens on the north and south sides of the rift and is mainly concentrated in the area with abrupt variations in the V_p/V_s ratios.

Conclusion

We imaged the crustal structure by using the receiver function H - κ stacking technique and obtained the results of the crustal thickness and average V_p/V_s ratio structures covering the Shanxi Rift and surrounding regions. The results show that the crustal thickness gradually increases from southeast to northwest in the research region. The Moho depth is positively correlated with altitude (isostasy coefficient is ~ 5.51), implying that there may be an exchange of crust–mantle materials beneath the Shanxi rift and its adjacent regions. The Yuncheng graben exhibits the strongest crustal thinning, followed by the Linfen and Taiyuan grabens, which indicates that the grabens in the Shanxi Rift have probably gradually developed from south to north. The average V_p/V_s ratios of the Yuncheng, Xinding, and Datong grabens in the north and south of the Shanxi Rift are higher than those of the Taiyuan and Linfen grabens in the central part, and the zones of densely distributed earthquakes are located in the abrupt belt of variation in the V_p/V_s ratio (in places with lower V_p/V_s ratios). We speculate that the possibility of strong earthquakes in the central Shanxi Rift is larger than that on the northern and southern sides.

Supplementary Information

The online version contains supplementary material available at <https://doi.org/10.1186/s40623-021-01528-8>.

Additional file 1: Figure S1. Synthetic receiver function with 1 km thick sedimentary layer and different κ value of sediment. The depth of Moho is 40 km and the average crustal V_p/V_s ratio (under sediment layer) is 1.78. (a) $\kappa = 2.0$. (b) $\kappa = 2.5$. (c) $\kappa = 3.0$. (d) $\kappa = 3.5$. **Figure S2.** H - κ Analysis of Synthetic receiver function in Figure S1. (a), (c), (e) and (g) is H - κ stacking of RF in Figure S1(a–d) without sediments. (b), (d), (f) and (h) is H - κ stacking of RF in Figure S1(a–d) with sediments. **Figure S3.** Synthetic receiver function with 2 km thick sedimentary layer and different κ value of sediment. The depth of Moho is 40 km and the average crustal V_p/V_s ratio (under sediment layer) is 1.78. (a) $\kappa = 2.0$. (b) $\kappa = 2.5$. (c) $\kappa = 3.0$. (d) $\kappa = 3.5$. **Figure S4.** H - κ Analysis of Synthetic receiver function in Figure S3. (a), (c), (e)

and (g) is H - κ stacking of RF in Figure S3(a-d) without sediments. (b), (d), (f) and (h) is H - κ stacking of RF in Figure S3(a-d) with sediments. **Figure S5.** Synthetic receiver function with 5 km thick sedimentary layer and different κ value of sediment. The depth of Moho is 40 km and the average crustal V_p/V_s ratio (under sediment layer) is 1.78. (a) $\kappa = 2.0$. (b) $\kappa = 2.5$. (c) $\kappa = 3.0$. (d) $\kappa = 3.5$. **Figure S6.** H - κ Analysis of Synthetic receiver function in Figure S3. (a) H - κ stacking of RF in Figure S5(a) without sediments. (b) H - κ stacking of RF in Figure S5(a) with sediments. **Figure S7.** (a) Distribution of sedimentary thickness and stations. (b-c) Receiver functions of stations 41210, 15782. **Figure S8.** - Analysis of stations 61133 and 61109. **Table S1.** Crustal thickness and V_p/V_s ratio beneath the stations in the study area. H : the estimated crustal thickness; κ : the V_p/V_s .

Acknowledgements

We thank the China Earthquake Administration for the seismic waveform data used in this study. We are grateful to two anonymous reviewers and Associate Editors Dr. Pascal Audet for their constructive reviews, which have greatly improved the presentation of this paper.

Authors' contributions

CJ, LS and CY carried out most of geologic investigation, data collection and pre-treatment. YZ, LX and SX contributed to data of the earthquake distribution in the study. CY and CJ analyzed the data and drafted the manuscript. All the authors read and approved the final manuscript.

Funding

This study was supported by National Key Research and Development Program of China (2017YFC1500103), National Natural Science Foundation of China (Grants 41704050) and the Fundamental Scientific Research Project of Institute of Geology, China Earthquake Administration (IGCEA2016).

Availability of data and materials

Seismic waveform data by China Seismic Array Data Management Center at Institute of Geophysics, China Earthquake Administration (<http://www.china-raydmc.cn/>, <https://doi.org/10.12001/ChinArray.Data>).

Declarations

Competing interests

The authors declare that they have no competing interests.

Author details

¹Lhasa National Geophysical Observation and Research Station, State Key Laboratory of Earthquake Dynamics, Institute of Geology, CEA, Beijing 10029, China. ²Guangdong Provincial Key Lab of Geodynamics and Geohazards, School of Earth Sciences and Engineering, Sun Yat-Sen University, Guangzhou 510275, China. ³Gansu Earthquake Agency, Lanzhou 730000, China.

Received: 17 June 2021 Accepted: 6 October 2021

Published online: 29 October 2021

References

- Ai S, Zheng Y, Riaz MS, Song M, Zeng S, Xie Z (2019) Seismic evidence on different rifting mechanisms in southern and northern segments of the Fenhe-Weihe Rift zone. *J Geophys Res Solid Earth* 124:609–630. <https://doi.org/10.1029/2018JB016476>
- Airy GB (1855) On the computation of the effect of the attraction of mountain masses, as disturbing the apparent astronomical latitude of stations in geodetic surveys. *Phil Trans Roy Soc (Lond)* B145:101–104
- Ammon CJ (1991) The isolation of receiver effects from teleseismic P waveforms. *Bull Seismol Soc Am* 81(6):2504–2510. <https://doi.org/10.1785/BSSA0810062504>
- Cai Y, Wu J, Rietbrock A, Wang W, Fang L, Yi S, Liu J (2021) S wave velocity structure of the crust and upper mantle beneath Shanxi rift, central North China Craton and its tectonic implications. *Tectonics* 40:e2020TC006239. <https://doi.org/10.1029/2020TC006239>
- Chang X, Liu YK, He JK, Sun HC (2007) Lower velocities beneath the Taihang mountains, northeastern China. *Bull Seismol Soc Am* 97:1364–1369. <https://doi.org/10.1785/0120060210>
- Chen X (1993) A systematic and efficient method of computing normal modes for multilayered half-space. *Geophys J Int* 115(2):391–409. <https://doi.org/10.1111/j.1365-246X.1993.tb01194.x>
- Chen L, Cheng C, Wei ZG (2009) Seismic evidence for significant lateral variations in lithospheric thickness beneath the central and western North China craton. *Earth Planet Sci Lett* 286(1–2):171–183. <https://doi.org/10.1016/j.epsl.2009.06.022>
- Cheng C, Chen L, Yao H, Jiang M, Wang B (2013) Distinct variations of crustal shear wave velocity structure and radial anisotropy beneath the North China Craton and tectonic implications. *Gondwana Res* 23:25–38. <https://doi.org/10.1016/j.jgr.2012.02.014>
- ChinArray (2006) China Seismic Array waveform data. China Earthquake Administration. <https://doi.org/10.12001/ChinArray.Data>
- Christensen NI, Fountain D (1975) Constitution of the lower continental crust based on experimental studies of seismic velocities in granulite. *Geol Soc Am Bull* 86(2): 227–236. Doi: [https://doi.org/10.1130/0016-7606\(1975\)86<227:COTLCC>2.0.CO;2](https://doi.org/10.1130/0016-7606(1975)86<227:COTLCC>2.0.CO;2)
- Christensen NI (1996) Poisson's ratio and crustal seismology. *J Geophys Res Solid Earth* 101:3139–3156. <https://doi.org/10.1029/95JB03446>
- Deng QD, Wang KL, Wang YP, Tang HY, Wu YW, Ding ML (1973) On the tendency of seismicity and the geological set-up of the seismic belt of Shanxi graben. *Sci Geol Sin* 1:37–47 (in Chinese)
- Deng QD, Cheng SP, Min W, Yang GZ, Ren DW (1999) Discussion on Cenozoic tectonics and dynamics of Ordos Block. *J Geomech* 5(3):13–22 (in Chinese)
- Farra V, Vinnik LP (2000) Upper mantle stratification by P and S receiver functions. *Geophys J Int* 141:699–712. <https://doi.org/10.1046/j.1365-246X.2000.00118.x>
- Guo LH, Meng XH, Shi L, Chen ZX (2012) Preferential filtering method and its application to Bouguer gravity anomaly of Chinese continent. *Chin J Geophys* 55(12):4078–4088. <https://doi.org/10.6038/j.issn.0001-5733.2012.12.020>
- Guo Z, Chen Y, Yin W (2015) Three-dimensional crustal model of Shanxi graben from 3D joint inversion of ambient noise surface wave and Bouguer gravity anomalies. *Chin J Geophys* 58(3):821–831. <https://doi.org/10.6038/cjg20150312>
- Hao M, Wang Q, Zhang P, Li Z, Li Y, Zhuang W (2021) "Frame wobbling" causing crustal deformation around the Ordos block. *Geophys Res Lett* 48:e2020GL091008. <https://doi.org/10.1029/2020GL091008>
- He RZ, Shang XF, Yu CQ, Zhang HJ, Van der Hilst R (2014) A unified map of Moho depth and V_p/V_s ratio of continental China by receiver function analysis. *Geophys J Int* 199:1910–1918. <https://doi.org/10.1093/gji/ggu365>
- Hu X, Cui X, Zhang G, Wang G, Arno Z, Shi B, Jiang D (2021) Analysis on the mechanical causes of the complex seismicity in Changning area. *China. Chin J Geophys* 64(1):1–17. <https://doi.org/10.6038/cjg202100232>
- Kearey P, Klepeis KA, Vine FJ (2009) Global tectonics, 3rd edn, vol 3. Wiley, Oxford, p 751
- Kind R, Yuan X, Saul J, Nelson D, Sobolev SV, Mechie J, Zhao W, Kosarev G, Ni J, Achauer U, Jiang M (2002) Seismic images of crust and upper mantle beneath Tibet: evidence for Eurasian plate subduction. *Science* 298:1219–1221. <https://doi.org/10.1126/science.1078115>
- Langston CA (1979) Structure under Mount Rainier, Washington, inferred from teleseismic body waves. *J Geophys Res Solid Earth* 84(B9):4749–4762. <https://doi.org/10.1029/JB084iB09p04749>
- Lei J (2012) Upper-mantle tomography and dynamics beneath the North China Craton. *J Geophys Res Solid Earth* 117(B6):6313. <https://doi.org/10.1029/2012JB009212>
- Li YL, Yang JC, Xia ZK, Mo DW (1998) Tectonic geomorphology in the Shanxi Graben System, northern China. *Geomorphology* 23:77–89. [https://doi.org/10.1016/S0169-555X\(97\)00092-5](https://doi.org/10.1016/S0169-555X(97)00092-5)
- Li C, Xu P, Sun Y, Jia J (2010) The Jinzhong transition belt and its geological significance by receiver function in Shanxi region. *Chin J Geophys* 53(5):1143–1148. <https://doi.org/10.3969/j.issn.0001-5733.2010.05.015>
- Li Z, Liu B, Yuan H, Feng S, Chen W, Li W, Kou K (2014) Fine crustal structure and tectonics of Linfen Basin from the results of seismic reflection profile. *Chin J Geophys* 57(5):1487–1497. <https://doi.org/10.6038/cjg20140513>

- Liu QY, Kind R, Li SC (1996) Maximal likelihood estimation and nonlinear inversion of the complex receiver function spectrum ratio. *Chin J Geophys* 39(4):500–511
- Liu M, Yang Y, Shen Z, Wang S, Wang M, Wan Y (2007) Active tectonics and intracontinental earthquakes in China: the kinematics and geodynamics. In: Stein S, Mazzotti S (Eds.), *Continental intraplate earthquakes: science, hazard, and policy issues*. Geological Society of America Special Paper, vol 425, pp 299–318. Doi: [https://doi.org/10.1130/2007.2425\(19\)](https://doi.org/10.1130/2007.2425(19))
- Liu QL, Wang CY, Yao ZX, Chang LJ, Lou H (2011) Study on crustal thickness and velocity ratio in mid-western Northern China Craton. *Chin J Geophys* 54(9):2213–2224. <https://doi.org/10.3969/j.issn.0001-5733.2011.09.003>
- Liu QY, Van der Hilst RD, Li Y, Yao HJ, Chen JH, Guo B, Qi SH, Wang J, Huang H, Li SC (2014) Eastward expansion of the Tibetan Plateau by crustal flow and strain partitioning across faults. *Nat Geosci* 7(5):361–365. <https://doi.org/10.1038/ngeo2130>
- Luo Y, Chong JJ, Ni SD, Chen QF, Chen Y (2008) Moho depth and sedimentary thickness in the capital region. *Chin J Geophys* 51:796–806
- Northrup C, Royden L, Burchfiel B (1995) Motion of the Pacific plate relative to Eurasia and its potential relation to Cenozoic extension along the eastern margin of Eurasia. *Geology* 23:719–722. [https://doi.org/10.1130/0091-7613\(1995\)023%3c0719:MOTPPR%3e2.3.CO;2](https://doi.org/10.1130/0091-7613(1995)023%3c0719:MOTPPR%3e2.3.CO;2)
- Olsen KH (1995) *Continental rifts: evolution, structure, tectonics*. Elsevier Science, Amsterdam
- Qu W, Lu Z, Zhang M, Zhang Q, Wang Q, Zhu W, Qu FF (2017) Crustal strain fields in the surrounding areas of the Ordos Block, central China, estimated by the least-squares collocation technique. *J Geodyn* 106:1–11. <https://doi.org/10.1016/j.jog.2017.01.005>
- Sengör A, Burke K (1978) Relative timing of rifting and volcanism on Earth and its tectonic implications. *Geophys Res Lett*. <https://doi.org/10.1029/GL005i006p00419>
- Shen ZK, Zhao CK, Yin A, Li YX, Jackson DD, Fang P, Dong DN (2000) Contemporary crustal deformation in East Asia constrained by global positioning system measurements. *J Geophys Res Solid Earth* 105(B3):5721–5734. <https://doi.org/10.1029/1999JB900391>
- Sheng SZ, Wan YG, Huang JC, Bu YF, Liang X (2015) Present tectonic stress field in the Circum-Ordos region deduced from composite focal mechanism method. *Chin J Geophys* 58(2):436–452. <https://doi.org/10.6038/cjg20150208>
- Shi W, Cen M, Chen L, Wang Y, Chen X, Li J, Chen P (2015) Evolution of the late Cenozoic tectonic stress regime in the Shanxi Rift, central North China Plate inferred from new fault kinematic analysis. *J Asian Earth Sci* 114:54–72. <https://doi.org/10.1016/j.jseae.2015.04.044>
- Song M, Zheng Y, Liu C, Li L, Wang X (2015) Shear-wave velocity structure of the crust and uppermost mantle in the Shanxi rift zone. *Earthq Sci* 28(2):135–149. <https://doi.org/10.1007/s11589-015-0117-0>
- Song MQ, Zheng Y, Ge C, Li B (2012) Relocation of small to moderate earthquakes in Shanxi Province and its relation to the seismogenic structures. *Chin J Geophys* 55(2):513–525. <https://doi.org/10.6038/j.issn.0001-5733.2012.02.014>
- Su P, He H, Tan X, Liu Y, Shi F, Kirby E (2021) Initiation and evolution of the Shanxi Rift System in North China: Evidence from low-temperature thermochronology in a plate reconstruction framework. *Tectonics* 40:e2020TC006298. <https://doi.org/10.1029/2020TC006298>
- Tang YC, Chen YJ, Zhou SY, Ning JY, Ding ZF (2013) Lithosphere structure and thickness beneath the North China craton from joint inversion of ambient noise and surface wave tomography. *J Geophys Res Solid Earth* 118:2333–2346. <https://doi.org/10.1002/jgrb.50191>
- Tang Y, Feng Y, Chen Y, Zhou S, Ning J, Wei S, Li P, Yu C, Fan W, Wang H (2010) Receiver function analysis at Shanxi Rift. *Chin J Geophys* 53(9):2102–2109. <https://doi.org/10.3969/j.issn.0001-5733.2010.09.010>
- Tapponnier P, Molnar P (1976) Slip-line field theory and large-scale continental tectonics. *Nature* 264(5584):319–324. <https://doi.org/10.1038/264319a0>
- Tapponnier P, Peltzer G, Le Dain AY, Armijo R, Cobbold P (1982) Propagating extrusion tectonics in Asia: new insights from simple experiments with plasticine. *Geology* 10(12):611–616. [https://doi.org/10.1130/0091-7613\(1982\)10%3c611:PETIAN%3e2.0.CO;2](https://doi.org/10.1130/0091-7613(1982)10%3c611:PETIAN%3e2.0.CO;2)
- Tapponnier P, Xu Z, Roger F, Meyer B, Aumaud N, Wittlinger G, Yang J (2001) Oblique stepwise rise and growth of the Tibet Plateau. *Science* 294:1671–1677. <https://doi.org/10.1126/science.105978>
- Teng JW, Wang FY, Zhao WZ, Zhao JR, Li M, Tian XB, Yan YF, Zhang YQ, Zhang CK, Duan YH, Yang ZX, Xu CF (2008) Velocity distribution of upper crust, undulation of sedimentary formation and crystalline basement beneath the Ordos basin in North China. *Chin J Geophys* 51(6):1753–1766
- Tian ZY, Han P, Xu KD (1992) The Mesozoic–Cenozoic East China rift system. *Tectonophysics* 208(1–3):341–363. <https://doi.org/10.1016/B978-0-444-89912-5.50025-9>
- Tian X, Teng J, Zhang H, Zhang Z, Zhang Y, Yang H, Zhang K (2011) Structure of crust and upper mantle beneath the Ordos Block and the Yinshan Mountains revealed by receiver function analysis. *Phys Earth Planet Inter* 184:186–193. <https://doi.org/10.1016/j.pepi.2010.11.007>
- Wang Y, Wang JY, Xiong LP, Deng JF (2001) Lithospheric geothermics of major geotectonic units in China mainland. *Acta Geosci Sin* 22:17–22 (in Chinese)
- Wang J, Liu Q, Chen J, Li S, Guo B, Li Y (2009) The crustal thickness and Poisson's ratio beneath the Capital Circle Region. *Chin J Geophys* 52(10):57–66
- Wang CY, Sandvol E, Zhu LP, Lou H, Yao ZX, Luo XH (2014) Lateral variation of crustal structure in the Ordos block and surrounding regions, North China, and its tectonic implications. *Earth Planet Sci Lett* 387:198–211. <https://doi.org/10.1016/j.epsl.2013.11.033>
- Wang WL, Wu J, Fang L, Lai G, Cai Y (2017) Sedimentary and crustal thicknesses and Poisson's ratios for the NE Tibetan Plateau and its adjacent regions based on dense seismic arrays. *Earth Planet Sci Lett* 462:76–85. <https://doi.org/10.1016/j.epsl.2016.12.040>
- Wang Y, Li Z, Ning J (2020) Spatial Distribution of Earthquakes and Crustal Seismic Velocity in Shanxi Rift Zone. *Acta Scientiarum Naturalium Universitatis Pekinensis*. 56(2):283–290. <https://doi.org/10.13209/j.0479-8023.2020.001> (in Chinese)
- Wei ZG, Chen L, Wang BY (2013) Regional variations in crustal thickness and Vp/Vs ratio beneath the central-western North China Craton and adjacent regions. *Geol J* 48:531–542. <https://doi.org/10.1002/gj.2473>
- Wu Y, Ding ZF, Wang XC, Zhu LP (2018) Crustal structure and geodynamics of the North China Craton derived from a receiver function analysis of seismic wave data. *Chin J Geophys* 61(7):2705–2718. <https://doi.org/10.6038/cjg2018L0244>
- Xu X, Ma X (1992) Geodynamics of the Shanxi Rift system. *China Tectonophysics* 208(1–3):325–340. [https://doi.org/10.1016/0040-1951\(92\)90353-8](https://doi.org/10.1016/0040-1951(92)90353-8)
- Xu X, Ma X, Deng Q (1993) Neotectonic activity along the Shanxi rift system. *China Tectonophysics* 219(4):305–325. [https://doi.org/10.1016/0040-1951\(93\)90180-R](https://doi.org/10.1016/0040-1951(93)90180-R)
- Yeck WL, Sheehan AF, Schulte-Pelkum V (2013) Sequential H-stacking to obtain accurate crustal thicknesses beneath sedimentary basins. *Bull Seismol Soc Am* 103(3):2142–2150. <https://doi.org/10.1785/0120120290>
- Yin A (2000) Mode of Cenozoic east-west extension in Tibet suggesting a common origin of rifts in Asia during the Indo-Asian collision. *J Geophys Res Solid Earth*. <https://doi.org/10.1029/2000JB900168>
- Yu Y, Song J, Liu KH, Gao SS (2015) Determining crustal structure beneath seismic stations overlying a low-velocity sedimentary layer using receiver functions. *J Geophys Res Solid Earth* 120:3208–3218. <https://doi.org/10.1002/2014JB011610>
- Yuan X, Kind R, Li X, Wang R (2006) The S receiver functions: synthetics and data example. *Geophys J Int* 165:555–564. <https://doi.org/10.1111/j.1365-246X.2006.02885.x>
- Zandt G, Ammon CJ (1995) Continental crust composition constrained by measurements of crustal Poisson's ratio. *Nature* 374:152–154. <https://doi.org/10.1038/374152a0>
- Zhang YQ, Mercier JL, Vergdly P (1998) Extension in the graben systems around the Ordos (China), and its contribution to the extrusion tectonics of south China with respect to Gobi-Mongolia. *Tectonophysics* 285:41–75. [https://doi.org/10.1016/S0040-1951\(97\)00170-4](https://doi.org/10.1016/S0040-1951(97)00170-4)
- Zhang YQ, Ma Y, Yang N, Shi W, Dong SW (2003) Cenozoic extensional stress evolution in North China. *J Geodyn* 36(5):591–613. <https://doi.org/10.1016/j.jog.2003.08.001>
- Zhang H, Huang Q, Zhao G, Guo Z, Chen Y (2016) Three-dimensional conductivity model of crust and uppermost mantle at the northern Trans North China Orogen: Evidence for a mantle source of Datong volcanoes. *Earth Planet Sci Lett* 453:182–192. <https://doi.org/10.1016/j.epsl.2016.08.025>
- Zhao GC, Cawood PA, Wilde SA, Lu LZ (2001) High-pressure granulites (retrograded eclogites) from the Hengshan Complex, North China Craton: petrology and tectonic implications. *J Petrol* 42:1141–1170. <https://doi.org/10.1093/petrology/42.6.1141>
- Zhao L, Zheng TY, Lu G, Ai YS (2011) No direct correlation of mantle flow beneath the North China Craton to the India-Eurasia collision: constraints

- from new SKS wave splitting measurements. *Geophys J Int* 187:1027–1037. <https://doi.org/10.1111/j.1365-246X.2011.05201.x>
- Zheng TY, Zhao L, Zhu RX (2009) New evidence from seismic imaging for subduction during assembly of the North China Craton. *Geology* 37:395–398. <https://doi.org/10.1130/G25600A.1>
- Zhu L, Kanamori H (2000) Moho depth variation in southern California from teleseismic receiver functions. *J Geophys Res Solid Earth* 105:2969–2980. <https://doi.org/10.1029/1999JB900322>

- Zhu RX, Xu YG, Zhu G, Zhang HF, Xia QK, Zheng TY (2012) Destruction of the North China Craton. *Sci China Earth Sci* 55(10):1565–1587. <https://doi.org/10.1007/s11430-012-4516-y>

Publisher's Note

Springer Nature remains neutral with regard to jurisdictional claims in published maps and institutional affiliations.

Submit your manuscript to a SpringerOpen[®] journal and benefit from:

- Convenient online submission
- Rigorous peer review
- Open access: articles freely available online
- High visibility within the field
- Retaining the copyright to your article

Submit your next manuscript at ► [springeropen.com](https://www.springeropen.com)
